EPJ Web of Conferences **268**, 00012 (2022) https://doi.org/10.1051/epjconf/202226800012
LNES 2021

Conceptual design of a water-cooled first wall component for a tokamak machine

Gabriele De Sano

Department of Industrial Engineering, University of Rome "Tor Vergata"
Via del Politecnico 1, 00133 Rome, Italy

Summary. — In a tokamak, the first wall is a barrier protecting the internal parts of the machine from the intense fluxes of heat and particles coming from the plasma. This contribution presents the critical issues of a water-cooled first wall component based on steel as structural material, that is a relevant case study for the design of future fusion power plants.

1. – Layout of an actively cooled first wall component

The exploitation of nuclear fusion for commercial electricity production is a promising solution to ensure the future energy needs, given its important advantages: the fuel is virtually unlimited and widely available, no greenhouse gases are produced, the process is intrinsically safe, and radioactive waste is recyclable after a relatively short time. Fusion reactions powering our Sun and the stars can be performed inside a device on Earth by creating a suitable environment for the fuel. The fusion process needs extremely high temperatures, on the order of 10 keV, thus the fuel exists in a plasma state enabling the positively charged nuclei to collide with each other and to react at a sufficiently high rate [1]. A potential architecture for a fusion reactor relies on the tokamak layout, namely a toroidally shaped device which is able to confine the hot plasma in a finite volume by

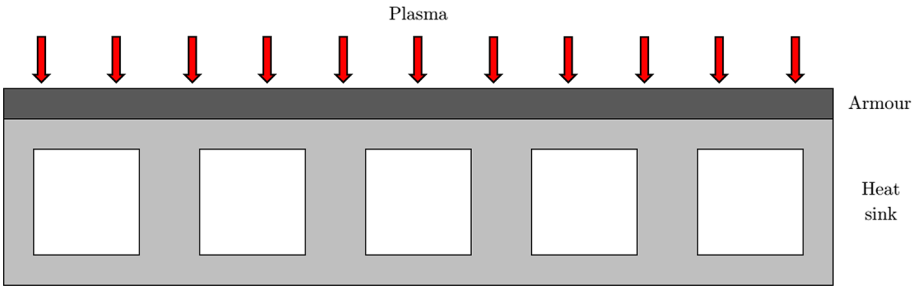

Fig. 1. – Cartoon schematic illustrating a possible layout of an actively cooled first wall component, with multiple rectangular cooling channels in the heat sink and a flat tile armour.

means of strong magnetic fields [2]. During the operation of a tokamak, heating power is continuously supplied to the plasma in order to maintain it at the necessary high temperatures and sustain the reactions. At steady state, the same amount of heat is emitted by the plasma and carried by fluxes of photons and charged particles, which interact with the surrounding elements of the tokamak. For this reason, the walls of the reaction chamber are covered by the so-called plasma facing components (PFCs), that exhaust the plasma heating power and shield the internal parts of the machine. Since a tokamak is characterized by a pulsed operation, PFCs are loaded only for periods of time. If the loads are applied for a few seconds, the effects of thermal inertia prevent materials from reaching their technological limits. However, all upcoming devices will operate with pulse lengths of hundreds or even thousands of seconds [3], thus it becomes mandatory for all PFCs to actively exhaust the thermal power by means of a cooling system. Water is frequently adopted as coolant.

The first wall, which is the main focus of the present contribution, consists of PFCs covering most of the plasma facing surface. The layout of an actively cooled first wall component consists of two main parts, namely the *armour* and the *heat sink*. The first is a layer directly facing the plasma, while the second is the structural material in which the cooling channels are manufactured (see fig. 1). For all PFCs, the need for an armour results from the interaction with charged particles, which collide with the surface layer of the walls causing sputtering, that is the ejection of atoms which then become impurities in the plasma. To date, tungsten (W) is the most promising candidate as plasma facing material because it shows a high energy threshold to sputtering and a resulting low erosion yield [4]. At the same time, neutrons produced by the reactions escape the plasma and penetrate deeply inside the whole reactor, damaging both functional and structural materials. Nuclear reactions with the nuclei can occur, leading to radioactivity. Moreover, high-energy neutrons can displace nuclei from their lattice positions and trigger a dislocation cascade. These phenomena are responsible for embrittlement and loss of strength in materials. The unit “displacement per atom” (dpa) is typically used to express lattice damage by neutrons and is defined as the number of times that an atom is displaced, on average, for a given neutron fluence.

TABLE I. – *Properties* (*at* 20 °C) *of some materials employed in PFCs* [5, 6].

	Coeff. of th. expansion α 10^{-6} [K^{-1}]	Young's modulus E [GPa]	Th. conductivity λ [$W\,m^{-1}\,K^{-1}$]	$\frac{\alpha E}{\lambda}$ 10^3 [$s\,m^{-2}$]
CuCrZr	16.7	128	318	6.7
Eurofer (Steel)	10.4	217	28	80.6
Tungsten	4.5	398	173	10.4

2. – Structural materials for the heat sink

The thermal power deposited on a PFC generates temperature gradients within the volume. The presence of temperature differences between two regions results in internal stress, since those regions elongate in a different way and undergo compression or traction. Considering a one-dimensional heat flow, a temperature difference across a material of thickness t depends both on the thermal conductivity λ of the material and the heat flux density q, according to Fourier's law of heat conduction:

$$\Delta T = \frac{tq}{\lambda}\,. \tag{1}$$

As a first approximation, the internal stress depends on the coefficient of thermal expansion α and Young's modulus E of the material, and increases for increasing ΔT:

$$\sigma \sim \alpha E \Delta T = \frac{\alpha E}{\lambda} tq. \tag{2}$$

Resulting from eq. (2), q has a direct impact on the internal stress, but it is linked to the applied heat load, which is fixed by tokamak operations and the precise location on the chamber walls. On the other hand, stress can be limited using materials with a reduced value of the factor $\frac{\alpha E}{\lambda}$. Table I compares the properties of some materials of interest, showing that the CuCrZr alloy is an excellent solution thanks to the high thermal conductivity λ of copper (Cu). In fact, CuCrZr is considered as the state-of-the-art material for the heat sink of a PFC. Unfortunately, its mechanical properties degrade even for a few dpa [7], after which the component shall be replaced, leading to high-radioactivity waste. The effects of neutron damage are negligible for current and upcoming experimental tokamaks, but they will be critical in the next step fusion device, the demonstration power plant DEMO [3], where a high neutron fluence is expected. DEMO will be the first fusion device to deliver electricity to the grid. Among other aims, DEMO should prove the economic feasibility of a fusion power plant, hence it is mandatory to limit the amount of waste [8] and minimize the substitution of components. Neutron resilient materials shall be developed in order to increase the lifetime of PFCs, particularly regarding the first wall that will be intensively bombarded by the high-energy fusion neutrons emitted

by the plasma [9]. Reduced Activation Ferritic/Martensitic (RAFM) steels represent a reliable candidate since they exhibit a high resistance to neutron damage and are characterized by advantageous low-activation properties. Eurofer, that is the selected material for DEMO, has proved to maintain acceptable mechanical properties up to a 80 dpa [10]. However, the use of steel leads to higher internal stress compared to Cu-based materials because of the lower λ, under the same geometry and heat flux. This fact could compromise the structural integrity of components, limiting the manageable power deposition.

Moreover, one must also compare the coefficients of thermal expansion α of the two materials used in the heat sink and the armour, since a difference in terms of thermal strain results in additional stress in the structure. As reported in table I, the α of bulk W is much smaller than that of the two heat sink materials. The resulting interface stress could lead to a failure of the structure-armour bond. In water-cooled PFCs, the use of W in both the heat sink and the armour is not viable because W behaves like a brittle material in the operating temperature range of water, thus it cannot perform a structural function as heat sink material.

3. – Preliminarily assessment of the internal stress in a first wall component

In this final section, the critical issues of a steel-based PFC are discussed on the basis of steady-state thermo-mechanical simulations in ANSYS Workbench Mechanical 2021 R1. A simple 2D geometry of the first wall component is considered, in order to arrive at a preliminarily and didactic analysis. It consists of a heat sink region surrounding a single water channel, with a deposited flat tile of armour facing the plasma. Eurofer and bulk W are employed in the two domains respectively, and their thermo-mechanical properties are taken from [5, 6]. As previously discussed, the internal stress in a PFC depends on the heat load. According to recent studies for DEMO [11], the heat flux deposited on the first wall at steady state remains everywhere below the value of $1\,\mathrm{MW\,m^{-2}}$, with conservative assumptions. The following parameters are assumed in the calculations:

- Operative water pressure: $p = 4\,\mathrm{MPa}$;
- Operative water bulk temperature: $T_{\mathrm{bulk}} = 70\,^{\circ}\mathrm{C}$;
- Water velocity: $u = 1\,\mathrm{m\,s^{-1}}$;
- Heat load deposited on the top surface of W: $q = 0.5\,\mathrm{MW\,m^{-2}}$.

The heat transfer between the Eurofer domain and the coolant is modelled by imposing T_{bulk} and the heat transfer coefficient. The latter can be evaluated through the Dittus-Boelter equation [12], that is a widely used correlation valid for turbulent forced convection. Once q and the heat transfer conditions are applied in the simulation, the temperature contours in the solid domains are obtained (see fig. 2). The temperature is maximum on the plasma facing surface and decreases as it approaches the fluid domain. The temperature gradient in Eurofer is higher than in W, since the λ of W is an order of magnitude larger.

Internal stresses are calculated after imposing the following loadings: operative water pressure in the cooling channel and temperature distribution in the solid domains. In

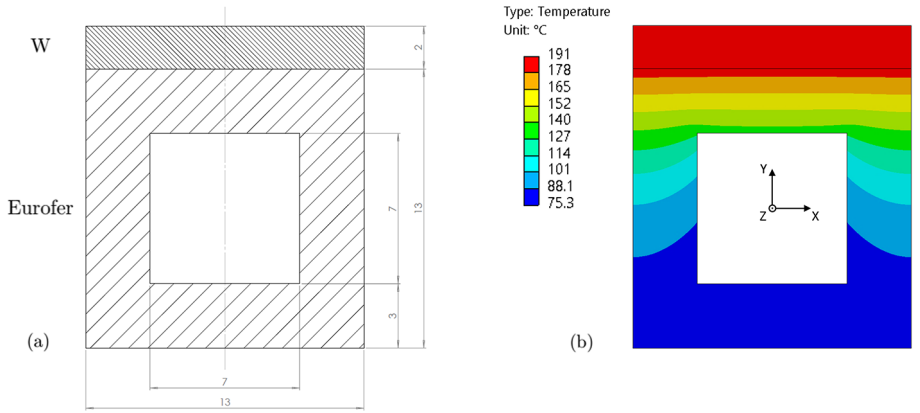

Fig. 2. – (a) 2D geometry of the model. (b) Temperature contours in the solid domains.

particular, water pressure is a mechanical load leading to primary stress P, while temperature gradients are a source of secondary stress Q. The thickness of the body along z is equal to 7 mm. The bottom face of the body is fixed in position along y ($U_y = 0$). On the left and right faces a coupling (U_x = constant) is imposed in order to simulate the presence of other channels in the first wall. Similarly, a coupling is imposed on the front and rear faces (U_z = constant) to model a longer component. The contours of von Mises stress [13] on the x-y plane are depicted in fig. 3, first considering the Eurofer domain only and then the whole geometry. As expected, stresses are higher in the second case because of the α mismatch between Eurofer and W, and the maximum values are concentrated in the region of the interface. The results are then verified to comply with the safety rules defined in the ITER Structural Design Criteria for In-vessel Components [5], that is a specific document developed for experimental tokamaks. The prescribed pro-

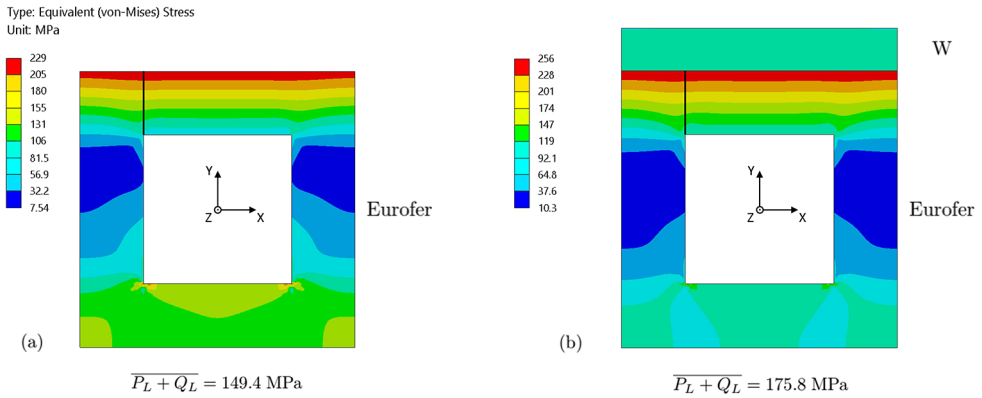

Fig. 3. – Contours of von Mises stress without (a) and with (b) the W domain. The average value used for the criterion is calculated on the black path.

cedure is to carry out the linearization of the von Mises stress along some critical paths through thicknesses of the component and to compare the calculated values with the allowable limits defined by the code. Below, the primary plus secondary stress criterion is discussed, being the most severe for this case study:

$$\overline{P_L + Q_L} \leq S_e \,, \tag{3}$$

$\overline{P_L + Q_L}$ is the average von Mises stress on a path resulting from both primary and secondary loadings. S_e is the allowable primary plus secondary stress intensity, strictly related to the material tensile strength but also dependent on the dpa level. $S_e \sim 200\,\text{MPa}$ is considered in [14] to be a conservative value, given the embrittlement due to neutron damage. The criterion is tested on the black path shown in fig. 3 since it exhibits the greater average stress intensity both without and with the W domain. The calculated value of $\overline{P_L + Q_L}$ is reported in fig. 3 for both cases and it is smaller than 200 MPa even with the W domain, thus the criterion is satisfied.

However, the magnitude of the internal stress will increase for a greater heat load at steady state, or during transient events when a larger power deposition is expected [11]. A possible solution to ensure structural integrity is to reduce the contribution of secondary stress by decreasing the material thickness t, according to eq. (2), but the primary stress due to the pressure loading increases for decreasing t, requiring a proper compromise. Moreover, the internal stress at the interface can be minimised realizing an interlayer to couple heat sink and armour. Functionally graded materials are currently under investigation for this application [15, 16], combining Eurofer and W with a properly engineered composition to compensate the α mismatch at the interface.

REFERENCES

[1] Romanelli F., *EPJ Web of Conferences*, **246** (2020) 00013.
[2] Wesson J., *Tokamaks*, third edition (Clarendon Press, Oxford) 2004.
[3] Donné T. *et al.*, *European Research Roadmap to the Realisation of Fusion Energy* (EUROfusion) 2018, ISBN: 978-3-00-061152-0.
[4] Neu R., *Tungsten as a Plasma Facing Material in Fusion Devices* (IPP 10/25) 2003, p. 12.
[5] *ITER Structural Design Criteria for In-vessel Components (SDC-IC)*, (ITER) 2012.
[6] Tavassoli F., *Fusion Demo Interim Structural Design Criteria (DISDC)/Appendix A: Material Design Limit Data/A3. S18E Eurofer Steel*, (CEA) 2004.
[7] Li M. *et al.*, *J. Nucl. Mater.*, **393** (2009) 36.
[8] Dose G. and Noce S., *EPJ Web of Conferences*, **246** (2020) 00014.
[9] Federici G. *et al.*, *Nucl. Fusion*, **57** (2017) 092002.
[10] van der Schaaf B. *et al.*, *J. Nucl. Mater.*, **386-388** (2009) 236.
[11] Maviglia F. *et al.*, *Nucl. Mater. Energy*, **26** (2021) 100897.
[12] Dittus F. W. and Boelter L. M. K., *Univ. Calif. Berkeley Publ. Eng.*, **2** (1930) 443.
[13] von Mises R., *Nachr. Akad. Wiss. Göttingen Math. Phys. Kl.*, **1** (1913) 582.
[14] Aiello G. *et al.*, *J. Nucl. Mater.*, **414** (2011) 61.
[15] Qu D. D. *et al.*, *Fusion Eng. Des.*, **98-99** (2015) 1389.
[16] Emmerich T. *et al.*, *Nucl. Fusion*, **60** (2020) 126004.